Advanced Scientific Instruments xxx (xxxx) xxx

Contents lists available at ScienceDirect

Advanced Scientific Instruments

journal homepage: www.keaipublishing.com/en/journals/asi/

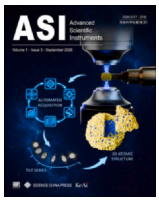

Research Article

A multifunctional plasma-assisted thin-film growth and *in-situ* transport characterization platform for quantum materials

Haotian Zhang[a,b,†], Weixuan Sun[a,c,†], Xiaodong Yu[a,c], Wei Hu[a], Jiquan Zhang[a], Qian Li[a], Xiao-Ping Ma[d], Huai-Xin Yang[d], Alejandro Silhanek[e], Ge He[b,*], Jie Yuan[a,c,**], Kui Jin[a,c,f,**]

[a] *Beijing National Laboratory for Condensed Matter Physics, Institute of Physics, Chinese Academy of Sciences, Beijing 100190, China*
[b] *School of Mechanical Engineering, Beijing Institute of Technology, Beijing 100081, China*
[c] *School of Physical Sciences, University of Chinese Academy of Sciences, Beijing 100049, China*
[d] *Institute of Physics, Chinese Academy of Sciences, Beijing 100190, China*
[e] *Experimental Physics of Nanostructured Materials, Department of Physics, University of Liège, Liège B-4000, Belgium*
[f] *Songshan Lake Materials Laboratory, Dongguan 523808, China*

ARTICLE INFO

Keywords:
Quantum materials
Pulsed laser deposition
Plasma-assisted growth
In-situ electrical transport

ABSTRACT

Quantum-material thin films are highly sensitive to growth conditions and surrounding chemical environments, motivating the development of integrated platforms that combine controlled synthesis with rapid property characterization. We present a multifunctional platform integrating three pulsed laser deposition chambers, a thermal evaporation chamber, radio-frequency plasma-assisted atmosphere regulation, vacuum sample transfer, and cryogen-free *in-situ* electrical transport characterization. The independently operated growth chambers achieve base pressures in the 10^{-8} Torr regime and accommodate a broad range of deposition pressures. In addition, laser-induced substrate temperatures up to 1000°C can be implemented. The *in-situ* transport system operates from 2.5 to 300 K and supports programmable multichannel resistance measurements over a nominal range from 1 mΩ to 1 MΩ. As a case study, a 60-nm-thick YBCO film was grown on MgO substrate and characterized, exhibiting a well-defined film–substrate interface, smooth surface morphology, and preferential *c*-axis-oriented growth. Its resistance–temperature dependence, measured *in situ* using the integrated transport system without breaking vacuum, shows a well-defined superconducting transition, demonstrating the capability of the system for reliable oxide thin-film growth and *in-situ* electrical characterization. The integrated platform provides a flexible experimental framework for controlled thin-film synthesis, plasma-assisted processing, and *in-situ* property investigation of quantum-material thin films.

1. Introduction

Quantum materials have attracted extensive interest owing to the emergence of diverse collective quantum states, including superconductivity,[1–3] charge- and spin-density waves (CDWs/SDWs),[4,5] topological phases,[6] and metal–insulator transitions.[7] The realization and manipulation of these quantum states often require precise control of composition, dimensionality, strain, interfaces, and defect concentrations.[8–10] Consequently, thin-film growth has become an indispensable approach for investigating emergent quantum phenomena and engineering novel functionalities. Recent advances in thin-film deposition techniques have enabled atomic-scale control of material synthesis, creating new opportunities to tailor electronic structures and stabilize quantum phases that are difficult to realize in bulk materials.[8–11]

The exploration of quantum materials relies critically on the availability to grow high-quality thin films with well-controlled crystal structures, stoichiometry, and defect distributions.[9,12,13] However, many quantum materials, particularly strongly correlated oxides, transition-metal chalcogenides, and low-dimensional heterostructures, exhibit pronounced sensitivity to growth conditions and surrounding

Peer review under the responsibility of Editorial Board of Advanced Scientific Instruments.
* Corresponding author.
** Corresponding authors at: Beijing National Laboratory for Condensed Matter Physics, Institute of Physics, Chinese Academy of Sciences, Beijing 100190, China.
E-mail addresses: ge.he@bit.edu.cn (G. He), yuanjie@iphy.ac.cn (J. Yuan), kuijin@iphy.ac.cn (K. Jin).
† These authors contributed equally to this paper.

https://doi.org/10.1016/j.asi.2026.100053
Received 16 September 2026; Received in revised form 26 October 2026; Accepted 28 October 2026

3117-3748/© 2026 The Authors. Publishing services by Elsevier B.V. on behalf of KeAi Communications Co. Ltd. This is an open access article under the CC BY license (http://creativecommons.org/licenses/by/4.0/).

Please cite this article as: H. Zhang, W. Sun, X. Yu et al., A multifunctional plasma-assisted thin-film growth and *in-situ* transport characterization platform for quantum materials, Advanced Scientific Instruments, https://doi.org/10.1016/j.asi.2026.100053

chemical environments. Even subtle variations in elemental composition, oxygen content, strain state, or defect density can significantly modify their structural, electronic, and magnetic properties.[9,12,14,15] Therefore, advanced thin-film growth platforms capable of precise synthesis control, flexible atmosphere regulation, and efficient *in-situ* characterization are increasingly important for the discovery, optimization, and investigation of novel quantum materials.

To meet these requirements, a variety of thin-film deposition techniques, including molecular beam epitaxy (MBE),[16,17] pulsed laser deposition (PLD),[18,19] and magnetron sputtering,[20] have been extensively developed for the synthesis of quantum materials. Among them, plasma-assisted deposition has emerged as a particularly attractive approach because it provides additional control over growth environments through the generation of reactive ions, radicals, and excited species.[13,20–23] The enhanced reactivity afforded by plasma sources expands the accessible growth parameter space, promotes nonequilibrium synthesis, and enables more flexible regulation of film-growth processes, thereby facilitating the synthesis of complex quantum materials with tailored functionalities.

Beyond precise control of thin-film growth, efficient exploration of quantum materials requires integrated platforms that directly connect synthesis with property characterization. Existing systems have combined thin-film growth with scanning tunneling microscopy, X-ray diffraction (XRD), photoemission spectroscopy, and electrical transport measurements, reducing sample handling and environmental exposure while enabling characterization of as-grown films.[24–28] Vacuum-connected configurations are particularly important for preserving surface and electronic properties during sample transfer.[27,29] However, the integration of multiple independently controlled growth environments, flexible atmosphere regulation, and rapid *in-situ* property evaluation remains technically challenging. Different material systems often require distinct deposition conditions and reactive environments, while samples must be transferred between growth and characterization stages without breaking vacuum. In addition, electrical transport characterization directly following growth is still less commonly incorporated than structural, microscopic, or spectroscopic probes.[24–27] These requirements motivate the development of a multi-chamber platform integrating independent growth environments, plasma-assisted atmosphere control, vacuum sample transfer, and *in-situ* electrical transport characterization.

In this work, we present a multifunctional platform for plasma-assisted quantum-material thin-film research that integrates a multi-chamber thin-film growth system, a plasma atmosphere regulation module, and an *in-situ* transport characterization system within an ultrahigh-vacuum environment. The multi-chamber architecture enables thin-film synthesis under independently controlled vacuum and atmosphere conditions while minimizing cross contamination between different growth processes. Chamber vacuum levels can be independently adjusted from 1×10^{-7} to 10^{-1} Torr, and substrate temperatures exceeding 1000°C can be achieved during growth. A plasma source with a maximum power of 500 W provides highly reactive growth atmospheres with reactive-species fluxes exceeding 1×10^{16} atoms cm^{-2} s^{-1}, offering enhanced flexibility for atmosphere regulation and process control. In addition, the integrated *in-situ* transport characterization module operates over a temperature range of 2.5–300 K, enabling rapid electrical-property measurements without exposing samples to ambient conditions. By combining flexible synthesis, plasma-assisted atmosphere control, and rapid property evaluation within a single platform, the system establishes an efficient framework for the synthesis, screening, and investigation of quantum-material thin films, while providing technological support for accelerated materials discovery and the construction of quantum-material databases.

2. General design

The platform integrates thin-film synthesis, plasma-assisted processing, vacuum sample transfer, and low-temperature electrical characterization within a single experimental infrastructure. This configuration enables quantum-material thin films to be grown, processed, and characterized sequentially without exposure to ambient conditions.

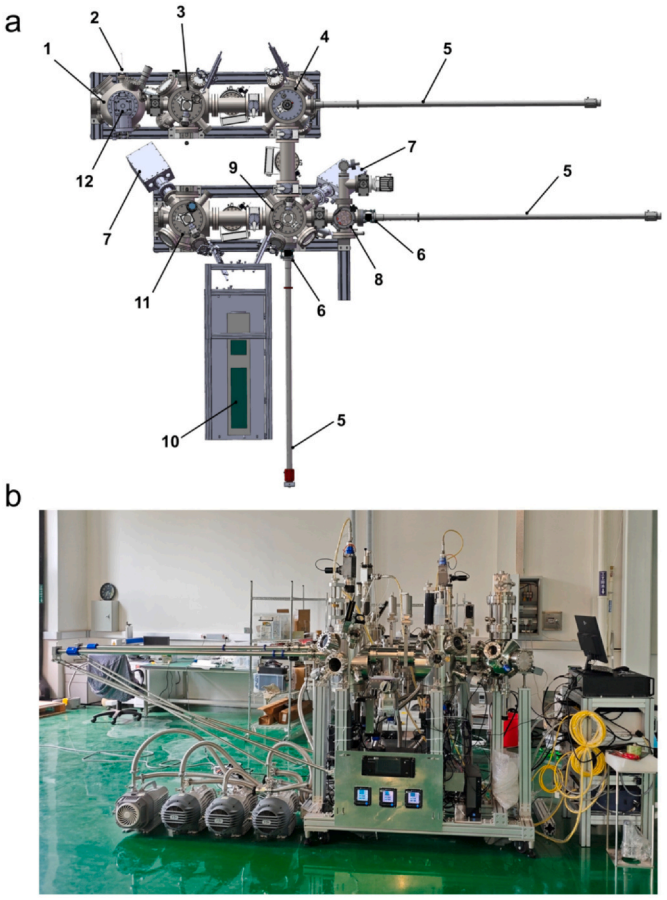

Fig. 1. Blueprint (a) and photograph (b) of the customized multi-chamber thin-film growth and characterization platform with integrated *in-situ* transport capability. The platform comprises an *in-situ* transport characterization chamber (1) equipped with a cryogen-free cryostat (12), an independent load-lock chamber (8), and four thin-film growth chambers, including three PLD chambers (4, 9, 11) and a thermal evaporation chamber (3). An RF plasma source (7) provides reactive species for plasma-assisted growth and processing, while the laser system (10) is used for PLD. Vacuum sample transfer is performed using a magnetically coupled transfer arm (5) equipped with a height-adjustment mechanism (6), together with a wobble stick (2), allowing sample holders to be manipulated and transferred between the interconnected chambers without breaking vacuum.

An overview of the system architecture is presented in Fig. 1. The platform comprises six primary functional chambers: three PLD chambers, a thermal evaporation chamber, an independent load-lock chamber, and an *in-situ* transport characterization chamber. The individual chambers are connected through a vacuum-transfer system that permits samples to be routed between different processing and characterization stages without breaking vacuum. The three PLD chambers can be operated independently to accommodate different material systems and deposition conditions, thereby reducing cross-contamination between dissimilar growth processes. The thermal evaporation chamber complements the PLD modules by enabling the deposition of metallic contacts, capping layers, and other essential auxiliary functional layers. An RF plasma source is integrated with the growth system to provide reactive species for plasma-assisted film growth and post-growth processing. Following deposition or plasma treatment, samples can be transferred directly to the transport characterization chamber for electrical measurements under vacuum.

The deposition chambers are independently pumped and isolated by ultrahigh-vacuum (UHV) gate valves, allowing the vacuum conditions and process atmospheres of the individual chambers to be controlled separately.

The operating pressure of each deposition chamber can be adjusted from 1×10^{-7} to 1×10^{-1} Torr, providing a broad pressure range for different thin-film growth environments. The measured base pressures of the three PLD chambers and the thermal evaporation chamber are approximately 7.1×10^{-8}, 1.9×10^{-8}, 2.4×10^{-8}, and 5.9×10^{-8} Torr, respectively, demonstrating stable operation in the 10^{-8} Torr regime.

Sample introduction and exchange are carried out through the dedicated load-lock chamber, which accommodates up to six sample holders and two deposition targets simultaneously. Starting from atmospheric pressure, the load-lock can be evacuated to approximately 6×10^{-7} Torr within 2 h. Samples and targets can therefore be introduced or exchanged without venting the main growth chambers, reducing disruption to ongoing experiments and preserving the base-vacuum conditions of the deposition system.

The *in-situ* transport characterization module is equipped with a cryogen-free cryostat driven by a high-power mechanical refrigerator and operates over a temperature range from 2.5 to 300 K. The temperature-control accuracy remains better than 0.1 K between 10 and 300 K. The transport chamber is separated from the growth system by a UHV gate valve and maintained by an independent pumping system, reaching a room-temperature base pressure of approximately 1.8×10^{-7} Torr. During sample exchange, the cryogenic stage is maintained near 15 K for approximately 1 h. Once the transfer procedure is completed, the system cools to its base temperature of 2.5 K within approximately 30 min. This arrangement allows low-temperature electrical characterization to follow thin-film growth while the sample remains under vacuum throughout the transfer process.

3. Chambers and transfer system

Fig. 2 shows the vacuum-transfer architecture and sample-handling scheme connecting the growth, processing, and characterization modules. The central transfer network allows samples and deposition targets to be routed between the load-lock, growth chambers, and transport characterization chamber without breaking vacuum. This arrangement enables sequential growth, processing, and electrical characterization while maintaining the sample under vacuum throughout the transfer procedure.

Sample handling is based on a flag-style sample holder used together with a cylindrical transfer holder, as illustrated in Fig. 2. Flag-style sample holders have been employed in integrated thin-film growth and characterization systems because they provide a compact and reproducible mechanical interface for sample positioning and inter-chamber transfer.[24] In the present system, the substrate is mounted on the flag-style holder, which remains the primary sample carrier during growth and transport characterization. For interchamber transfer, the flag-style holder is inserted into the cylindrical transfer holder. The cylindrical holder is engaged by the fork at the end of the magnetically coupled transfer arm and provides a common mechanical interface for transferring both sample holders and deposition targets through the vacuum system.

Samples and targets are introduced through the load-lock chamber shown in the lower-right part of Fig. 2, which accommodates up to six sample holders and two deposition targets simultaneously. After evacuation, the magnetically coupled transfer arm retrieves the selected transfer holder and delivers it to the required growth, processing, or characterization chamber. Fine vertical alignment between the transfer arm and the chamber ports is provided by a Z-translation mechanism at the chamber interface, facilitating reproducible engagement and release of the transfer holder during docking. The entire transfer sequence is therefore performed under vacuum without exposing the sample surface to ambient conditions.

The sample-loading configuration in the PLD chamber is illustrated in the enlarged view through viewport W4. The transfer holder is

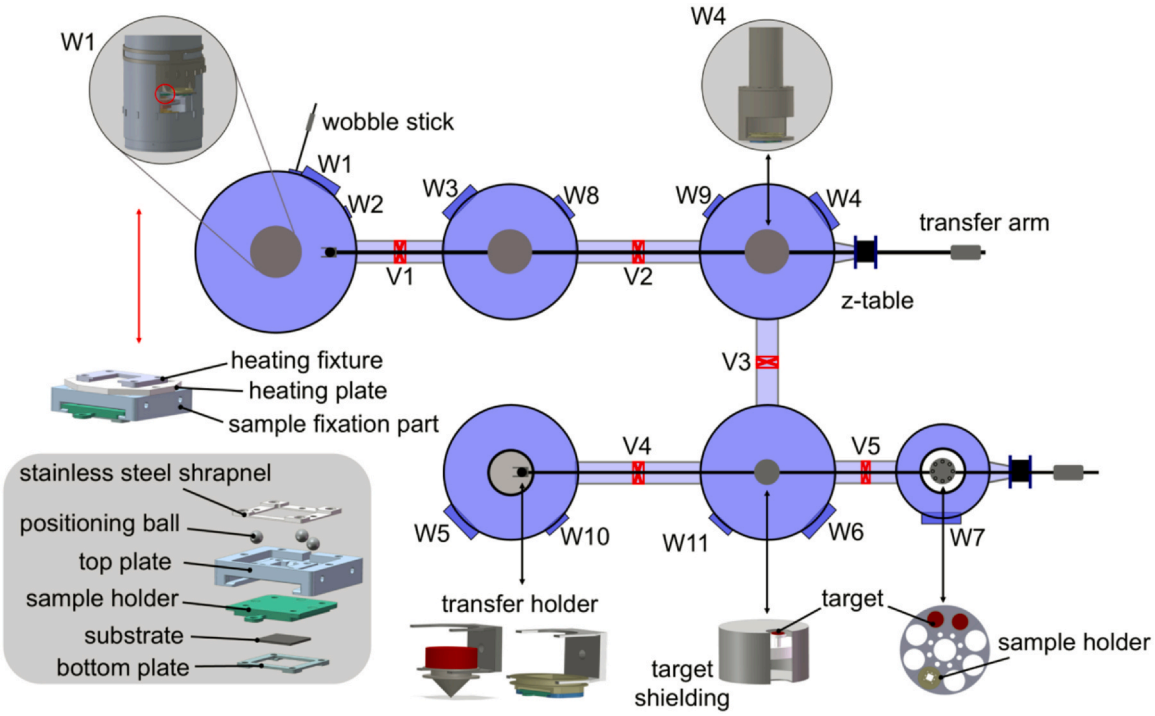

Fig. 2. Schematic layout of the vacuum-transfer system of the multi-chamber thin-film growth and characterization platform. The transfer network includes an *in-situ* transport characterization chamber (left), a thermal evaporation chamber (upper center), a PLD growth chamber (upper right), a PLD chamber (lower center), and a load-lock chamber (lower right), interconnected through gate valves V1–V5. Viewports W1–W8 provide visual access for sample-transfer and growth operations, while optical windows W9–W11 provide laser access to the PLD chamber. Samples and targets are transported between chambers using a magnetically coupled transfer arm equipped with a transfer holder. In the PLD chamber, the sample is positioned on a vertically movable heating stage, as illustrated in the enlarged view through viewport W4. For *in-situ* transport characterization, the sample is first delivered to a sample rack outside the radiation shield and is subsequently inserted into the cryogenic measurement position using a wobble-stick manipulator, as illustrated in the enlarged view through viewport W1. The lower-left inset shows an exploded view of the flag-style sample-holder assembly.

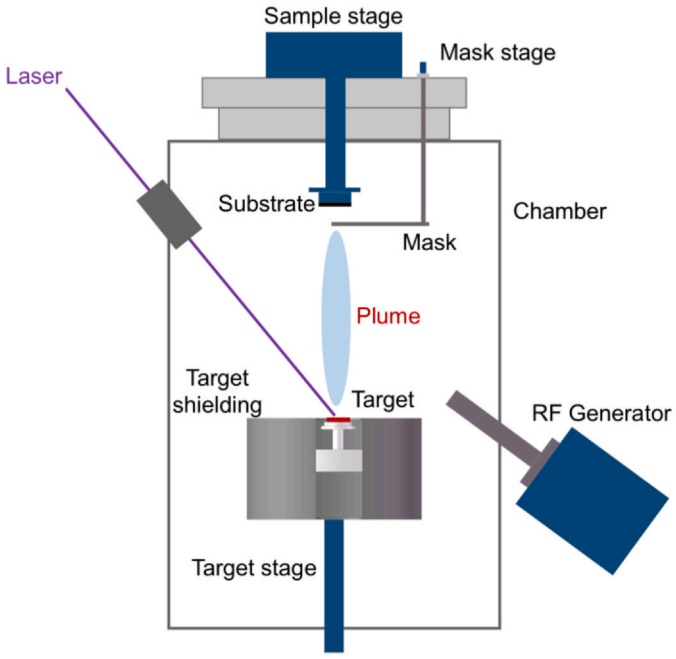

Fig. 3. Schematic illustration of the PLD growth chamber and associated processing components. The chamber incorporates a PLD laser beam delivery system, a target manipulator, a substrate stage equipped with laser heating and infrared temperature monitoring, a shadow mask, and an RF plasma source. Laser ablation of the target generates a plume directed toward the substrate, while the RF plasma source supplies activated species for plasma-assisted film growth and surface processing.

delivered to the growth chamber by the magnetically coupled transfer arm and aligned with the substrate stage. The sample is then positioned on a vertically movable heating stage that provides the required positioning and thermal control during deposition. After growth, the sample can be retrieved through the same transfer path and directed either to another processing chamber or to the transport characterization module.

Transfer into the transport characterization chamber requires an additional handling step, as illustrated in the enlarged view through viewport W1. The cylindrical transfer holder is first delivered to a sample rack located outside the radiation shield. A wobble-stick manipulator then removes the flag-style sample holder from the cylindrical holder and inserts it into the cryogenic measurement stage inside the radiation shield. Following electrical characterization, the sample holder can be returned to the cylindrical transfer holder and transferred back to a growth or processing chamber through the same vacuum-transfer network. This reversible transfer scheme permits repeated growth, processing, and transport measurements on the same sample without intermediate exposure to air.

The flag-style sample-holder assembly is shown in the lower-left inset of Fig. 2. It consists of a top plate, a bottom plate, positioning balls, and stainless-steel retaining clips. The positioning balls provide reproducible mechanical registration during repeated loading operations, while the retaining clips secure the substrate in the holder. Together with the cylindrical transfer holder, this modular design allows the same sample to be handled throughout the platform without remounting, reducing unnecessary manipulation and the associated risks of surface contamination and mechanical damage.

4. Film growth system

The thin-film growth modules are based on PLD and integrate a growth chamber, substrate manipulator, target manipulator, laser beam delivery and adjustment system, gas-handling components, and an RF plasma source, as schematically illustrated in Fig. 3. Their coordinated operation provides independent control over substrate position and temperature, target motion, laser irradiation, process atmosphere, and plasma-assisted surface reactions during deposition.

The substrate manipulator provides continuous 360° rotation and a vertical travel range of ± 50 mm. The vertical motion allows the substrate position and target-to-substrate distance to be adjusted for different deposition geometries, while continuous rotation can be used to improve the azimuthal uniformity of film growth. Substrate heating is provided by a non-contact laser-heating system, with the temperature monitored in real time using an infrared pyrometer. This configuration avoids direct electrical connections to the heated stage and is compatible with film growth over a broad range of vacuum and reactive-gas conditions.

The PLD laser is coupled to the growth chamber through an adjustable optical system in which a focusing lens is mounted on a motorized translation stage. Translation of the lens along the optical axis changes the focusing condition and hence the laser spot size at the target surface, allowing the incident laser fluence to be adjusted for different target materials and ablation conditions. This optical arrangement provides reproducible control of the laser irradiation conditions and facilitates optimization of the ablation process.

The target manipulator combines independent rotational and orbital motions through a dual-axis drive system. The orbital motion is driven by a servo motor and can be programmed for target selection and scanning over an extended area, while simultaneous rotation distributes successive laser pulses over the target surface. The combined motion reduces localized target erosion and improves utilization of the available target area during repeated deposition. A linear translation stage with a travel range of 100 mm provides an additional degree of freedom for target positioning and, in combination with the vacuum-transfer system, permits target exchange without venting the growth chamber. The multi-axis target manipulation system therefore supports sequential deposition from different targets and the preparation of multilayer or compositionally complex thin-film structures.

The growth chamber is further equipped with a movable shutter, a shadow mask, and controlled gas-injection lines. Before film deposition, the shutter can be closed while the target is pre-ablated, preventing material released during target conditioning from reaching the substrate. The process-gas flow is regulated using mass flow controllers (MFCs), allowing the gas composition and chamber pressure to be adjusted over the range from 10^{-3} to 10 Pa. Together with the independently pumped chamber, this gas-handling system provides flexible control of the reactive atmosphere required for different material systems.

A distinctive feature of the growth platform is the integration of an RF plasma source with the PLD chamber. The source, a commercial PCS-RF plasma source (SPECS Surface Nano Analysis GmbH, Germany), operates at powers of up to 500 W and provides a reactive-species flux exceeding 1×10^{16} atoms cm^{-2} s^{-1}. Unlike conventional PLD, in which the chemical activity of the background gas is governed primarily by gas pressure and plume–gas interactions, the RF plasma source activates the introduced gas and supplies additional reactive species to the substrate surface. The plasma conditions can therefore be adjusted independently of the laser-ablation parameters, introducing an additional degree of control over the growth environment. This configuration is particularly useful when enhanced surface reactivity is required for incorporation of reactive elements or stabilization of the desired film composition. More broadly, plasma assistance extends the accessible PLD growth window for oxide, nitride, and other functional thin films by providing an additional means of controlling gas-phase activation and surface reaction processes.

5. *In-situ* transport characterization system

A dedicated low-temperature transport characterization module is integrated with the thin-film growth platform to enable electrical

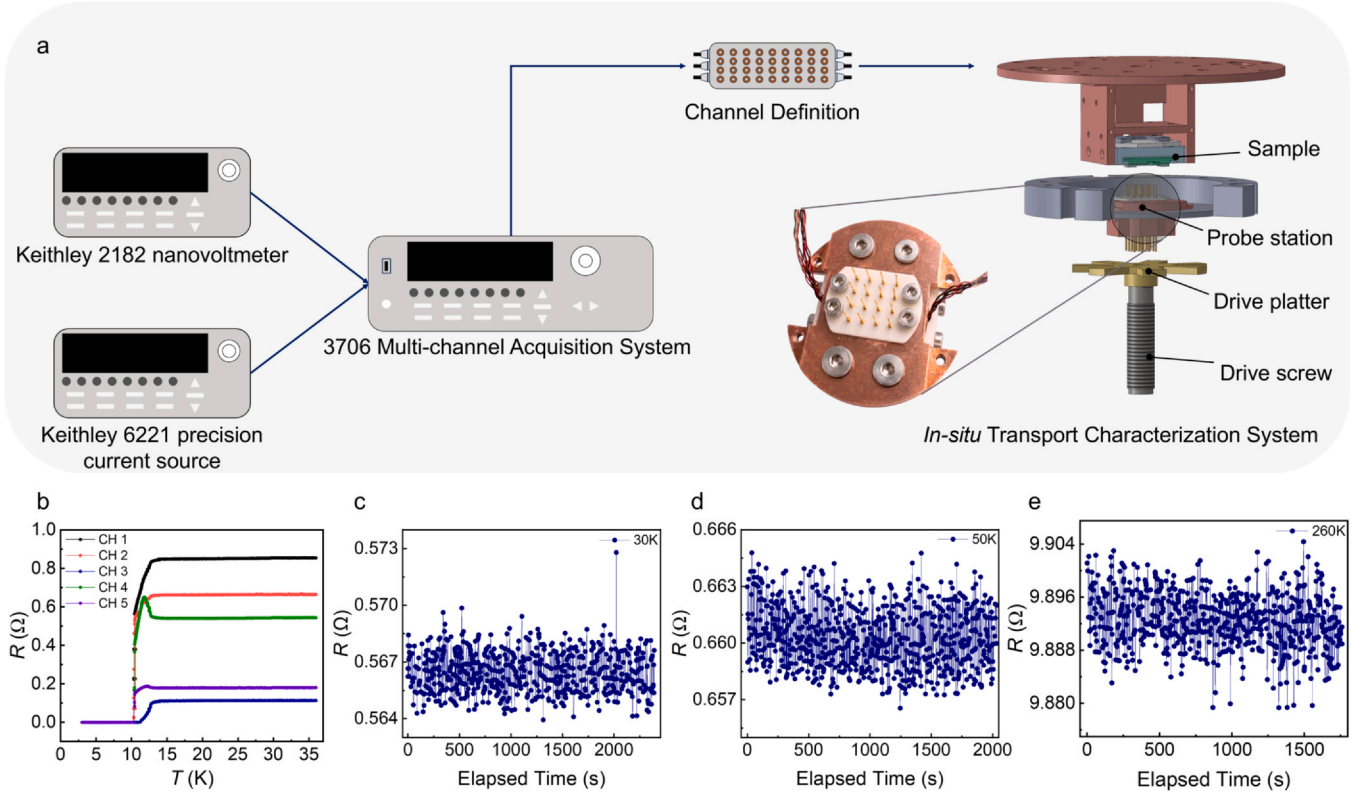

Fig. 4. *In-situ* transport characterization system and representative performance measurements. (a) Schematic illustration of the cryogenic multichannel transport characterization system integrated with the spring-probe array. (b) Resistance–temperature curves measured at five different positions on a combinatorial YBCO thin film using a single Keithley 6221/2182 measurement pair and a programmable switching matrix. (c–e) Representative resistance stability measurements performed at 30, 50, and 260 K, respectively, illustrating stable electrical measurements over a broad temperature range.

measurements without exposing the sample to ambient conditions. The system employs a closed-cycle Gifford–McMahon (GM) cryocooler as the primary refrigeration source and provides a temperature range from 2.5 to 300 K without the consumption of liquid helium. The transport chamber is connected to the growth system through a vacuum interconnection flange and can be pumped independently, allowing samples to be transferred directly from the growth chambers to the measurement stage while remaining under vacuum.

Electrical contact with the sample is established using a customized 16-pin spring-probe array. Similar spring-loaded probe arrays have been used for multichannel transport measurements of thin-film samples.[30] In the present system, the probe assembly is driven vertically by a screw mechanism located within the innermost thermal shield. The driving screw is supported by bearings and rotated using a wobble stick that engages a paddle through the sample transfer window, thereby driving the entire probe assembly vertically. This arrangement enables gradual adjustment of the probe position and contact pressure during engagement with the sample. Locating the drive mechanism inside the innermost shield avoids direct mechanical coupling to the outer shields and chamber body, thereby reducing parasitic thermal conduction. The spring-loaded probes accommodate controlled compression during contact, allowing the applied pressure to be adjusted while reducing the risk of excessive mechanical loading and sample damage.

The electrical routing architecture is shown schematically in Fig. 4a. A Keithley 3706 switching and acquisition system serves as the central routing unit. Two high-density switching modules provide 192 programmable switching channels, corresponding to 96 channel pairs for excitation and voltage sensing. Of these, 48 channel pairs are connected to a Keithley 6221 precision current source and the remaining 48 channel pairs to a Keithley 2182 nanovoltmeter. The 16 probe terminals inside the vacuum chamber are connected through electrical feedthroughs and a customized signal-routing module to the programmable switching matrix, allowing the excitation and voltage-sensing paths to be assigned to selected probe positions without manual rewiring.

The switching matrix is controlled through customized measurement software that integrates channel selection, excitation-current control, temperature monitoring, and resistance acquisition. Different probe configurations can therefore be defined programmatically according to the sample geometry and measurement requirements, enabling simultaneous or sequential transport measurements at multiple positions on the same sample.

The performance of the transport system was evaluated using representative multichannel resistance measurements. As shown in Fig. 4b, five R–T curves were acquired at different positions on a combinatorial YBCO thin film during a single temperature sweep. The measurements were performed sequentially using one Keithley 6221/2182 pair through the programmable switching matrix. The differences in resistance values and temperature dependences reflect the substantial spatial inhomogeneity of the combinatorial film. During measurement, the excitation current can be adjusted between 1 and 100 μA according to the sample resistance. The system covers a nominal resistance range from 1 mΩ to 1 MΩ. Representative resistance stability measurements obtained at 30, 50, and 260 K are shown in Fig. 4c–e, respectively. The small temporal variation of the resistance signals at these representative temperatures confirms stable electrical operation under the tested conditions.

6. System performance

Having described the film-growth and *in-situ* transport-characterization subsystems, we further demonstrate the practical capability of the integrated platform through the growth and characterization of a 60-nm-thick YBCO film on an MgO substrate. YBCO was selected as a representative material because of its complex multicomponent crystal

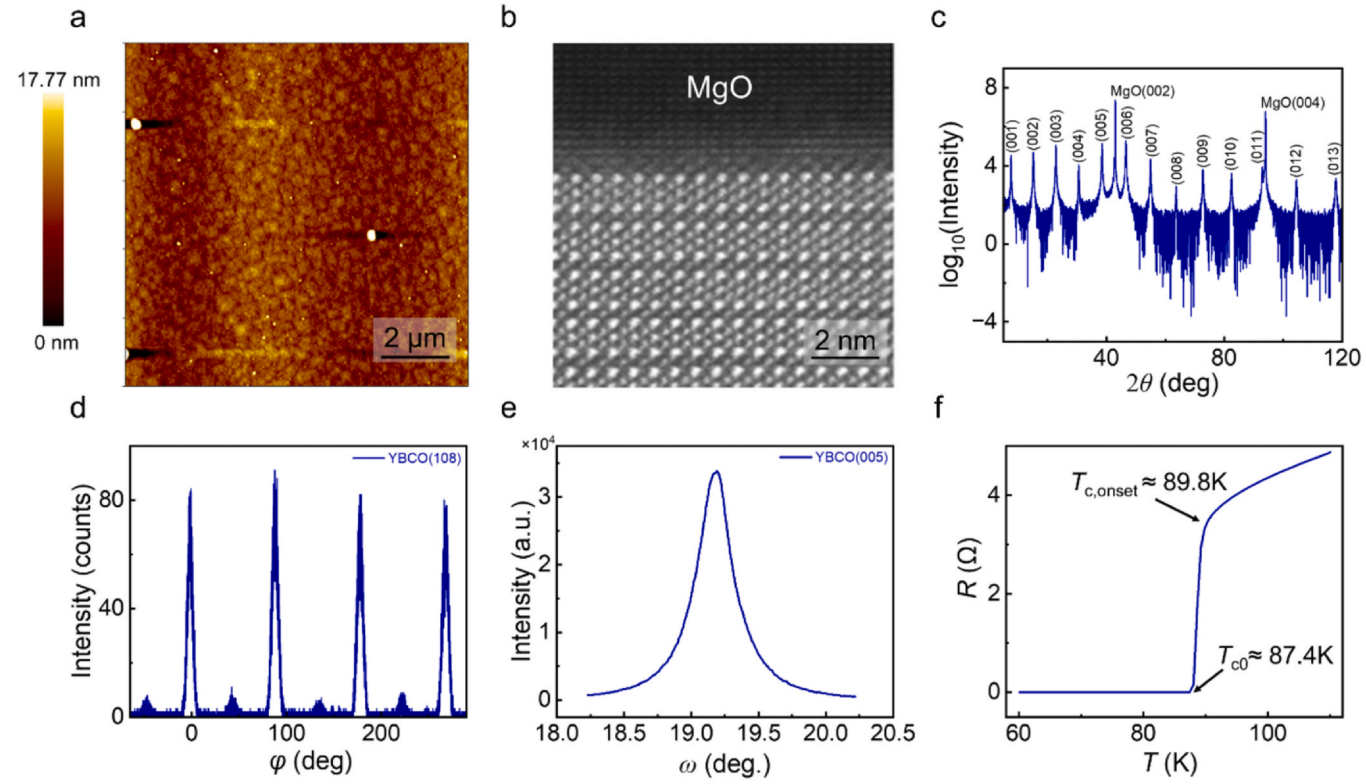

Fig. 5. Structural, morphological, and electrical characterization of a 60-nm-thick YBCO film grown on MgO using the integrated platform. (a) AFM surface topography. (b) Cross-sectional high-resolution TEM image of the YBCO/MgO interface. (c) Wide-range out-of-plane XRD scan. (d) In-plane φ-scan of the YBCO(108) reflection. (e) Rocking curve of the YBCO(005) reflection. (f) *In-situ* resistance–temperature measurement showing the superconducting transition.

structure and the pronounced sensitivity of its structural and superconducting properties to growth conditions, particularly cation stoichiometry and oxygen content. Fig. 5 summarizes its structural and morphological characteristics together with the resistance–temperature behavior measured *in situ* using the transport characterization system integrated into the platform. These measurements provide a direct evaluation of both the thin-film growth capability and the *in-situ* electrical characterization capability of the system.

The YBCO film was grown by pulsed laser deposition at a substrate temperature of 760°C and a deposition pressure of 0.2 Torr. The laser fluence and repetition rate were 4 J cm^{-2} and 1 Hz, respectively. Following deposition, the film was annealed at 500°C under a pressure of 1 bar O_2 for 1 h.

The surface morphology and local structural quality of the YBCO/MgO film were examined by atomic force microscopy (AFM) and transmission electron microscopy (TEM), respectively. The AFM topography shown in Fig. 5a, acquired over a 10 μm × 10 μm area, yields a root-mean-square surface roughness of $R_q = 1.82$ nm, indicating a relatively smooth film surface. The cross-sectional high-resolution TEM image (Fig. 5b) reveals an atomically abrupt YBCO/MgO interface and an ordered local lattice structure. Quantitative analysis of the interface profile over a lateral distance of 20 nm gives a root-mean-square interface roughness of $\sigma = 0.4$ nm, indicating interface fluctuations well below 1 nm.

The crystalline structure and orientation of the YBCO/MgO film were further examined by XRD, as shown in Fig. 5c–e. The wide-range 2θ scan (Fig. 5(c) exhibits a series of YBCO(00*l*) reflections together with the MgO substrate peaks, indicating preferential *c*-axis-oriented growth without prominent secondary-phase reflections within the detection limits of the measurement. The in-plane φ-scan of the YBCO (108) reflection (Fig. 5(d) shows four dominant peaks separated by approximately 90°, indicating a well-defined in-plane orientation. Weaker peaks between the dominant reflections suggest the presence of a small fraction of twin domains. The rocking curve of the YBCO(005) reflection Fig. 5(e) yields a full width at half maximum of approximately 0.31°, narrower than the value of 0.81° reported for YBCO/MgO films by Sanchez Cornejo *et al.*.[31] Although the film thicknesses and growth conditions differ between the two studies, this comparison indicates a relatively narrow out-of-plane orientation distribution in the present film. These diffraction results, together with the TEM observations, demonstrate that the platform can provide suitable conditions for the growth of structurally oriented YBCO thin films.

The electrical transport behavior of the same YBCO/MgO film was characterized *in situ* using the transport measurement system integrated into the platform, as shown in Fig. 5f. Following film growth, the sample was transferred under vacuum to the transport characterization chamber, allowing the resistance–temperature dependence to be measured without exposure to ambient conditions. The resistance decreases continuously upon cooling in the normal state and subsequently exhibits a pronounced superconducting transition, with a midpoint transition temperature of approximately 88.7 K and a near-zero-resistance temperature of approximately 87.4 K. These results are comparable to those reported for YBCO films of similar thickness. Danerud *et al.*[32] reported a zero-resistance temperature of 86.4 K for a 50-nm-thick laser-deposited YBCO film on MgO, while Arpaia *et al.*[33] demonstrated superconducting behavior in 50-nm-thick PLD-grown YBCO films on MgO(110). Although differences in substrate orientation, growth conditions, and transition-temperature criteria should be considered, these results demonstrate superconducting properties comparable to those of previously reported YBCO films of similar thickness. This measurement not only confirms the superconducting behavior of the grown YBCO film, but also directly demonstrates the capability of the platform to perform *in-situ* electrical transport characterization following thin-film growth without breaking vacuum.

Taken together, the TEM, AFM, XRD, and *in-situ* electrical transport measurements provide complementary validation of the integrated platform. The 60-nm-thick YBCO/MgO film exhibits an ordered local lattice structure, a well-defined film–substrate interface, a smooth

surface morphology, preferential *c*-axis orientation, and a clear superconducting transition. These results demonstrate that the platform can integrate controlled thin-film synthesis, vacuum sample transfer, and *in-situ* electrical transport characterization within a unified experimental system, providing a versatile basis for the preparation and investigation of quantum-material thin films.

7. Conclusions

In summary, we have developed a multifunctional platform integrating multi-chamber thin-film growth, plasma-assisted processing, vacuum sample transfer, and cryogen-free *in-situ* electrical transport characterization. The system incorporates three independently operated PLD chambers and a thermal evaporation chamber, with base pressures in the 10^{-8} Torr regime and substrate temperatures above 1000°C. An RF plasma source provides an additional means of controlling the reactive growth environment, while the dedicated load-lock and vacuum-transfer system enable samples to be processed and transferred between functional chambers without exposure to ambient conditions. The integrated transport module operates from 2.5 to 300 K and supports programmable multichannel resistance measurements over a nominal range from 1 mΩ to 1 MΩ.

The performance of the integrated platform was demonstrated using a 60-nm-thick YBCO film grown on an MgO substrate. TEM, AFM, and XRD measurements reveal a well-defined film–substrate interface, a smooth surface morphology, and preferential *c*-axis-oriented growth. Following deposition, the sample was transferred under vacuum to the transport characterization chamber, where a clear superconducting transition was observed in the resistance–temperature measurement. These results demonstrate the coordinated operation of the growth, plasma-assisted processing, vacuum-transfer, and *in-situ* transport modules, establishing the platform as an integrated experimental system for the preparation and investigation of quantum-material thin films. The modular architecture of the platform allows further functional expansion. Future upgrades will focus on automating sample positioning and probe engagement, introducing programmable masks for combinatorial thin-film growth, and improving the mechanical stability of the cryogenic transport system. These developments will provide a foundation for high-throughput synthesis, characterization, and data-driven optimization of quantum materials.

Author contributions

Jin K and Yuan J conceived the project. Yu X and Sun W developed and tested the experimental system. Yuan J, Jin K, He G, Li Q, and Yu X conceived the experiments. Hu W and Zhang J grew the material samples and performed the XRD and electrical transport measurements. Ma XP and Yang HX performed the TEM and AFM measurements. Jin K, Yuan J, He G, Zhang H and Silhanek A analyzed the experimental data. Zhang H, He G and Yuan J wrote the manuscript with comments from all the authors.

Declaration of Competing Interest

The authors declare that they have no known competing financial interests or personal relationships that could have appeared to influence the work reported in this paper.

Acknowledgments

We thank Prof. Qing Huan for his valuable discussions and support. This work is supported by the National Key R&D Program of China (Grant Nos. 2022YFA1603903, 2021YFA0718700 and 2024YFF0727103), the National Natural Science Foundation of China (Grant Nos. U23A6015, 12225412, 12474473 and 52588301), and the CAS Project for Young Scientists in Basic Research (Grant No. 2022YSBR-048).

References

1. Keimer B, Kivelson SA, Norman MR, Uchida S, Zaanen J. From quantum matter to high-temperature superconductivity in copper oxides. *Nature.* 2015;518:179–186.
2. Jin K, Butch NP, Kirshenbaum K, Paglione J, Greene RL. Link between spin fluctuations and electron pairing in copper oxide superconductors. *Nature.* 2011;476:73–75.
3. Puphal P, Schäfer T, Keimer B, Hepting M. Superconductivity in infinite-layer and Ruddlesden–Popper nickelates. *Nat Rev Phys.* 2026;8:70–85.
4. Teng X, Chen L, Ye F, et al. Discovery of charge density wave in a kagome lattice antiferromagnet. *Nature.* 2022;609:490–495.
5. He G, Shen J, Xie S, et al. Anisotropic electronic correlations in the spin density wave state of $La_3Ni_2O_7$. *Nat Commun.* 2026;17:6272.
6. Ren Y, Qiao Z, Niu Q. Topological phases in two-dimensional materials: a review. *Rep Prog Phys.* 2016;79:066501.
7. Imada M, Fujimori A, Tokura Y. Metal-insulator transitions. *Rev Mod Phys.* 1998;70:1039–1263.
8. Mannhart J, Schlom DG. Oxide interfaces—an opportunity for electronics. *Science.* 2010;327:1607–1611.
9. Hwang HY, Iwasa Y, Kawasaki M, Keimer B, Nagaosa N, Tokura Y. Emergent phenomena at oxide interfaces. *Nat Mater.* 2012;11:103–113.
10. Schlom DG, Chen L-Q, Pan X, Schmehl A, Zurbuchen MA. A thin film approach to engineering functionality into oxides. *J Am Ceram Soc.* 2008;91:2429–2454.
11. Basov DN, Averitt RD, Hsieh D. Towards properties on demand in quantum materials. *Nat Mater.* 2017;16:1077–1088.
12. Li J, Yang X, Zhang Z, Yang W, Duan X, Duan X. Towards the scalable synthesis of two-dimensional heterostructures and superlattices beyond exfoliation and restacking. *Nat Mater.* 2024;23:1326–1338.
13. Singh B, Fischer T, Mathur S. Field-enhanced chemical vapor deposition: new perspectives for thin film growth. *J Mater Chem A.* 2025;13:20104–20142.
14. Liu C, Liu T, Zhang Z, et al. Understanding epitaxial growth of two-dimensional materials and their homostructures. *Nat Nanotechnol.* 2024;19:907–918.
15. Santra P, Ghaderzadeh S, Ghorbani-Asl M, Komsa H-P, Besley E, Krasheninnikov AV. Strain-modulated defect engineering of two-dimensional materials. *npj 2D Mater Appl.* 2024;8:33.
16. Chambers SA. Epitaxial growth and properties of thin film oxides. *Surf Sci Rep.* 2000;39:105–180.
17. Chambers SA. Epitaxial growth and properties of doped transition metal and complex oxide films. *Adv Mater.* 2010;22:219–248.
18. Willmott PR, Huber JR. Pulsed laser vaporization and deposition. *Rev Mod Phys.* 2000;72:315–328.
19. Ashfold MNR, Claeyssens F, Fuge GM, Henley SJ. Pulsed laser ablation and deposition of thin films. *Chem Soc Rev.* 2004;33:23–31.
20. Anders A. Tutorial: Reactive high power impulse magnetron sputtering (R-HiPIMS). *J Appl Phys.* 2017;121:171101.
21. M.A. Lieberman, A.J. Lichtenberg. Principles of plasma discharges and materials processing. (2005).
22. Ostrikov K, Mehdipour H. Energy and matter-efficient size-selective growth of thin quantum wires in a plasma. *Appl Phys Lett.* 2011;98:033104.
23. Ostrikov K, Neyts EC, Meyyappan M. Plasma nanoscience: from nano-solids in plasmas to nano-plasmas in solids. *Adv Phys.* 2013;62:113–224.
24. He G, Wei Z, Feng Z, et al. Combinatorial laser molecular beam epitaxy system integrated with specialized low-temperature scanning tunneling microscopy. *Rev Sci Instrum.* 2020;91:013904.
25. Lee JH, Tung IC, Chang S-H, et al. *In-situ* surface/interface x-ray diffractometer for oxide molecular beam epitaxy. *Rev Sci Instrum.* 2016;87:013901.
26. Horiba K, Ohguchi H, Kumigashira H, et al. A high-resolution synchrotron-radiation angle-resolved photoemission spectrometer with *in situ* oxide thin film growth capability. *Rev Sci Instrum.* 2003;74:3406–3412.
27. Cui W, Zheng C, Zhang L, et al. An *in situ* electrical transport measurement system under ultra-high vacuum. *Rev Sci Instrum.* 2020;91:063902.
28. Orgiani P, Chaluvadi SK, Chalil SP, et al. Dual pulsed laser deposition system for the growth of complex materials and heterostructures. *Rev Sci Instrum.* 2023;94:033903.
29. Rutkowski MM, McNicholas KM, Zeng Z, Brillson LJ. Design of an ultrahigh vacuum transfer mechanism to interconnect an oxide molecular beam epitaxy growth chamber and an x-ray photoemission spectroscopy analysis system. *Rev Sci Instrum.* 2013;84:065105.
30. Jin K, Suchoski R, Fackler S, et al. Combinatorial search of superconductivity in Fe-B composition spreads. *APL Mater.* 2013;1:042101.
31. Sanchez Cornejo H, De Los Santos Valladares L, Barnes CHW, Moreno NO, Bustamante Dominguez A. Texture and magnetic anisotropy of $Yba_2Cu_3O_{7-\delta}$ film on MgO substrate. *J Mater Sci Mater Electron.* 2020;31:21108–21117.
32. Danerud M, Winkler D, Lindgren M, et al. Nonequilibrium and bolometric photoresponse in patterned $YBa_2Cu_2O_{7-\delta}$ thin films. *J Appl Phys.* 1994;76:1902–1909.
33. Arpaia R, Golubev D, Baghdadi R, et al. Transport properties of ultrathin $YBa_2Cu_2O_{7-\delta}$ nanowires: a route to single-photon detection. *Phys Rev B.* 2017;96:064525.